Supplementary Material for

Dioxygen Atom Co-doping g-C_3N_4 for Boosted Photoreduction Activity of CO_2 and Mechanism Investigation

Zhang Jiang[a,b], Mingnv Guo[c], Zhongqing Yang[a,b*], Ruiming Fang[a,b], Ziqi Wang[a,b], and Jingyu Ran[a,b]

a. Key Laboratory of Low-grade Energy Utilization Technologies and Systems, Chongqing University, Ministry of Education, Chongqing, 400044, China

b. School of Energy and Power Engineering, Chongqing University, Chongqing, 400044, China

c. School of Mechanical and Power Engineering, Chongqing University of Science and Technology, Chongqing, 401331, China

*Corresponding Author: Prof. Zhongqing Yang, E-mail address: zqyang@cqu.edu.cn

Table of Contents

1. Catalytic Characterization

In this study, the structure characterization of the catalyst in this experiment was obtained by the following five characterization methods. The X-ray diffraction (XRD) map of the catalyst sample was obtained by an X-ray diffractometer (D8 Advance, BRUKER, Germany) to study the crystalline form, phase and crystallinity of the catalyst with the excitation source Cu Kα ray (wavelength λ = 1.5406 Å) and a wide-angle scanning range of 10-90º. Fourier transform infrared spectroscopy is obtained by the Fourier transform infrared spectrometer (iS10 FT-IR spectrometer, NICOLET, USA) to analyze the chemical structure, chemical bonds and functional groups of the catalyst, the scanning range and resolution are 400-4000 cm^{-1} and 4 cm^{-1}, the signal-to-noise ratio is 50000:1, and the scanning is 32 times. X-ray photoelectron spectroscopy (XPS) is obtained by the X-ray photoelectron spectrometer (Escalab 250 Xi, THERMO FISCHER, USA) to detect the surface element composition, atomic valence state, valence band spectrum and content of the catalyst, and the contaminated carbon on the surface during XPS testing is used for calibration (C1s: 284.8 eV). Scanning electron microscopy (SEM) images and elemental distribution images (EDS) are obtained by field emission scanning electron microscopy (Su-8010, HITACHI, Japan) to observe the surface morphology and microstructure of the catalyst and the

distribution of elements, before the determination, a small amount of catalyst powder is dipped in conductive tape, pasted on the sample table, gold spray 30-60 s after the machine vacuum test, magnification of 10,000 to 100,000 times. UV-Vis DRS spectroscopy is obtained by UV-Vis spectrophotometer (Lambda 950, PERKINELMER, USA) to analyze the light absorption performance and bandgap width structure information of the catalyst, with a scanning range of 200-800 nm and a scanning speed of 20 $nm \cdot min^{-1}$.

The characterization of the photoelectric properties of the catalyst in this experiment was obtained by the following two characterization methods. Photoluminescence spectroscopy (PL) is obtained by a steady-state/transient fluorescence spectrometer (FLS 1000, EDINBURGH INSTRUMENTS, UK) to detect the separation of photogenerated carriers (electron-hole pairs) with an excitation wavelength of 388 nm and an emission band of 400-800 nm. The photocurrent-time response (I-t) was obtained by the Electrochemical Workstation (CHI-760E, Chenhua, China) to study the separation and recombination of photogenerated electron hole pairs under the same lighting conditions, with currents ranging from ±10 pA to ±0.25 pA.

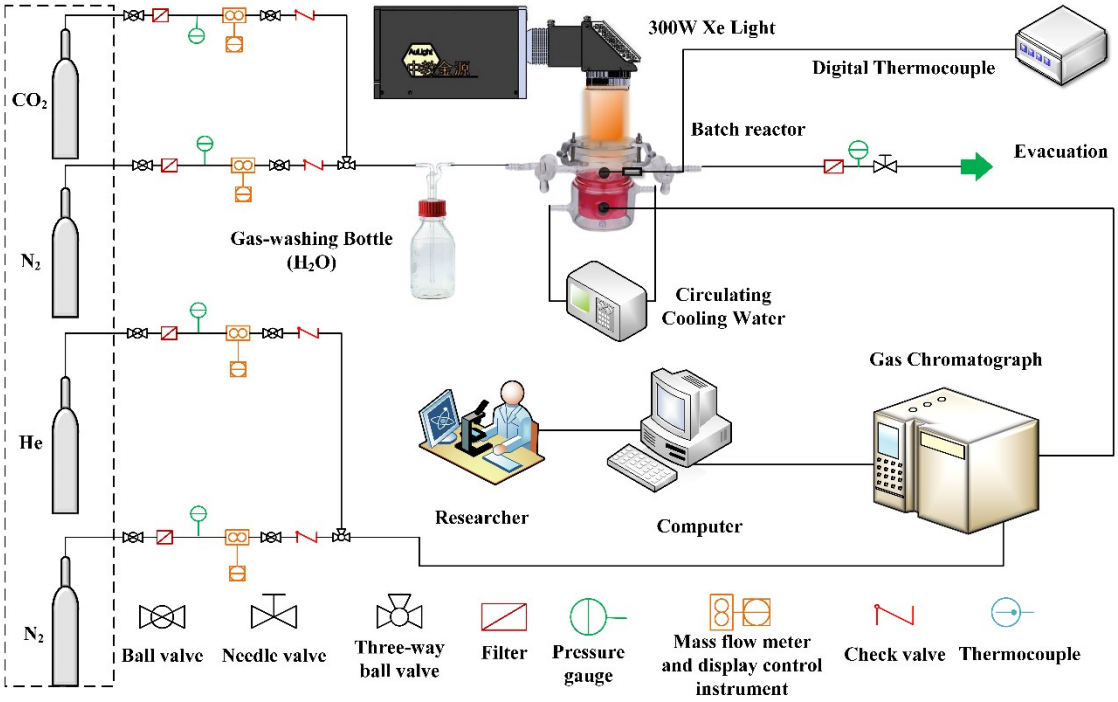

Fig. S1 Schematic diagram of photocatalytic CO_2 reaction system

2. Part of the experiment and characterization results

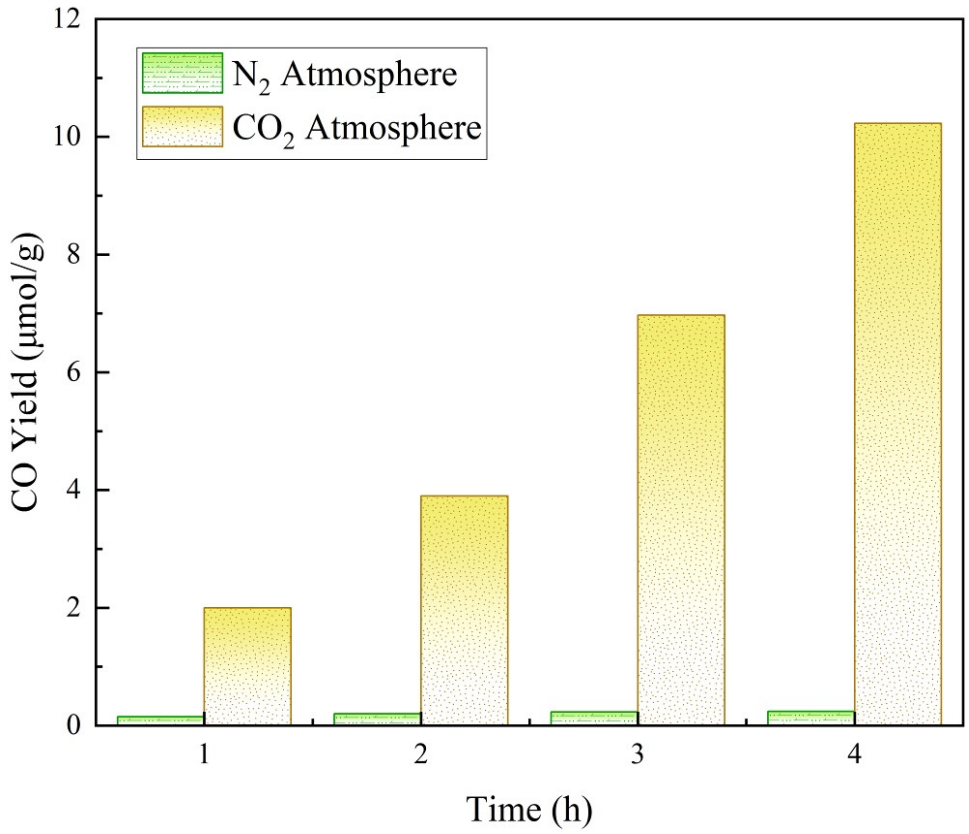

Fig. S2 Controlled experimental results

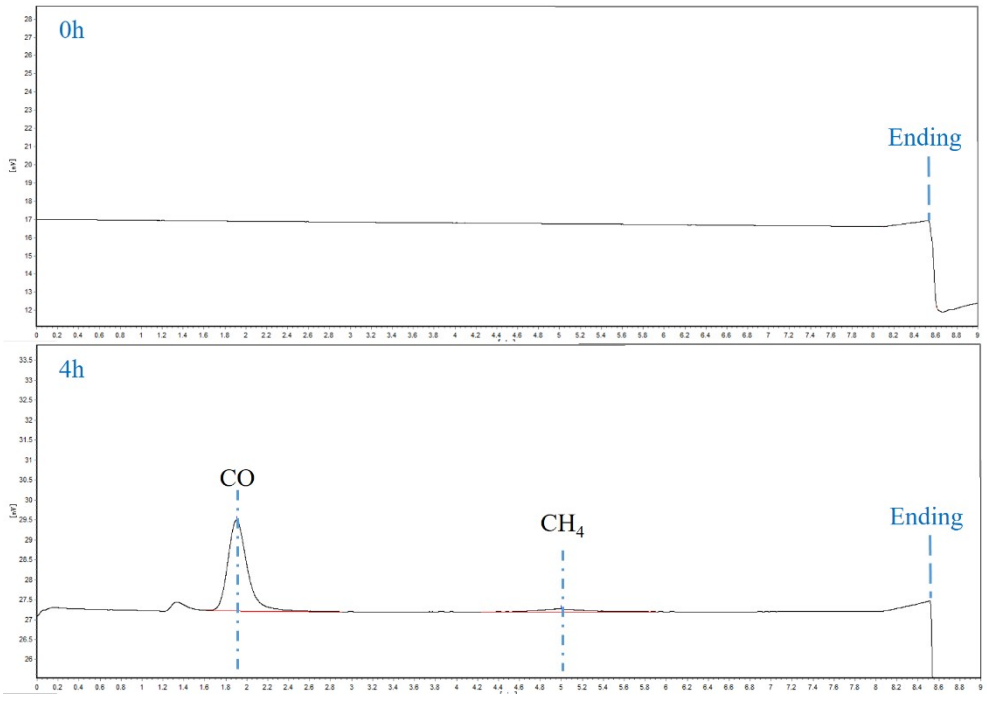

Fig. S3 GC raw data graph of cyclic stability experiment results at 0h and 4h

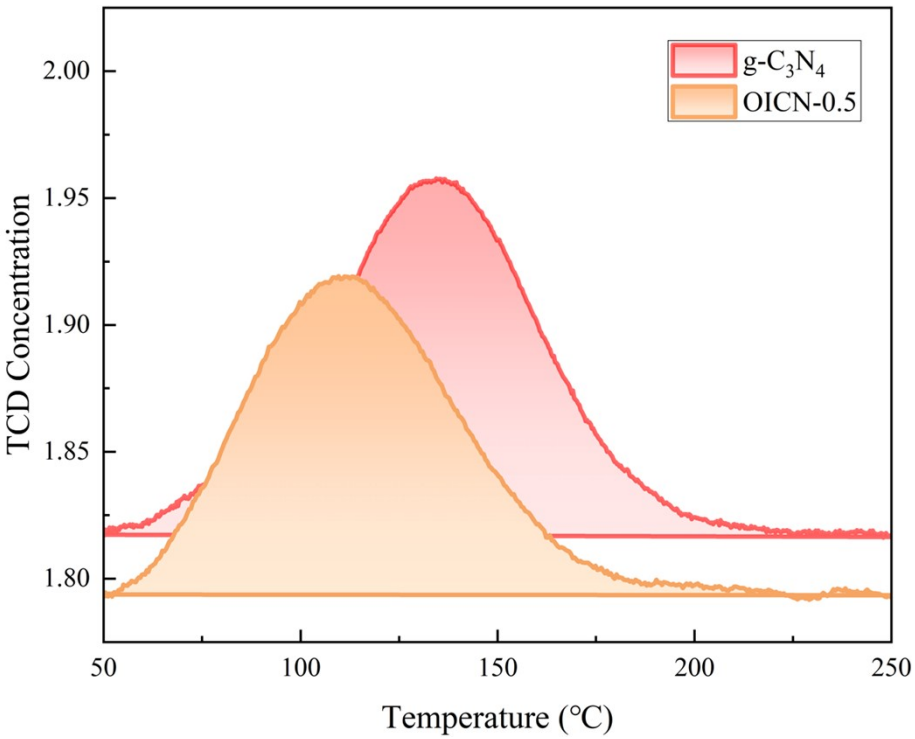

Fig. S4 CO_2-TPD results for g-C_3N_4 and OICN-0.5

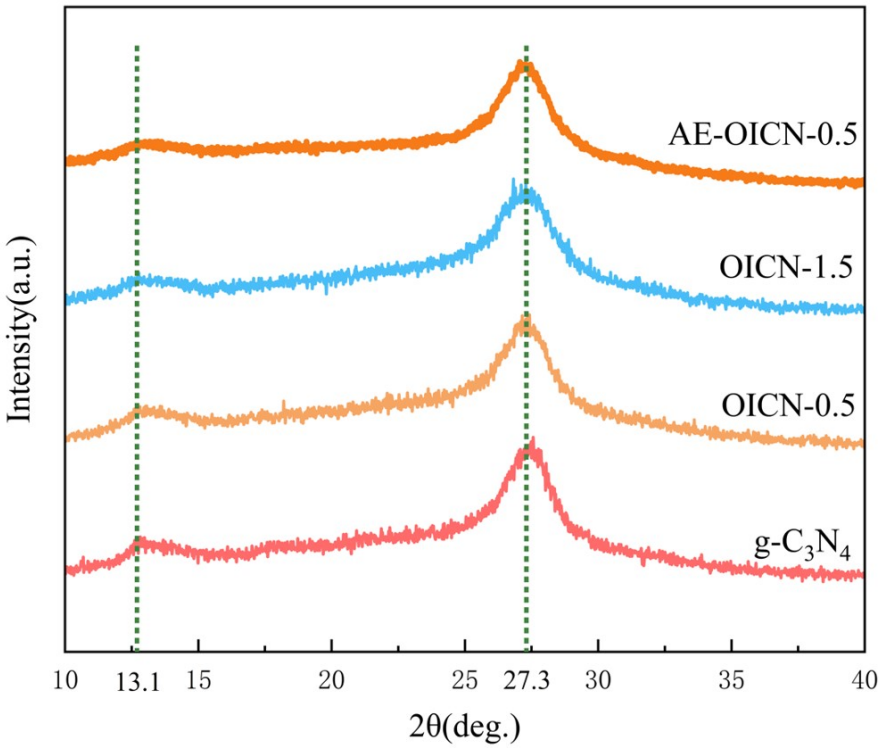

Fig. S5 XRD images of OICN-0.5 catalyst after photocatalysis experiment and catalysts before photocatalysis experiment

3. Density Functional Theory (DFT) Calculations

Here are the calculated parameters, the oxygen atom doped system and the gas molecular adsorption system were calculated by using the CASTEP (Cambridge Serial Total Energy Package) module in Materials Studio software for first-principle calculation, and the PBE function in the generalized gradient approximation GGA (Generalized Gradient Approximation) was used to deal with the exchange correlation among electrons. Ultrasoft Pseudopotential is used to describe the relationship between valence electrons and ionic reals. In geometric optimization, the convergence standard values for self-consistent iterative energy, atomic stress, stress, and atomic displacement are set to 1.0×10^{-5}eV/atom, 0.03eV/Å, 0.05GPa, and 0.001Å, respectively, and the plane wave truncation energy value is set to 380eV, and the k-mesh is set to 3×3×1.

The configuration diagram of doping sites is as follows.

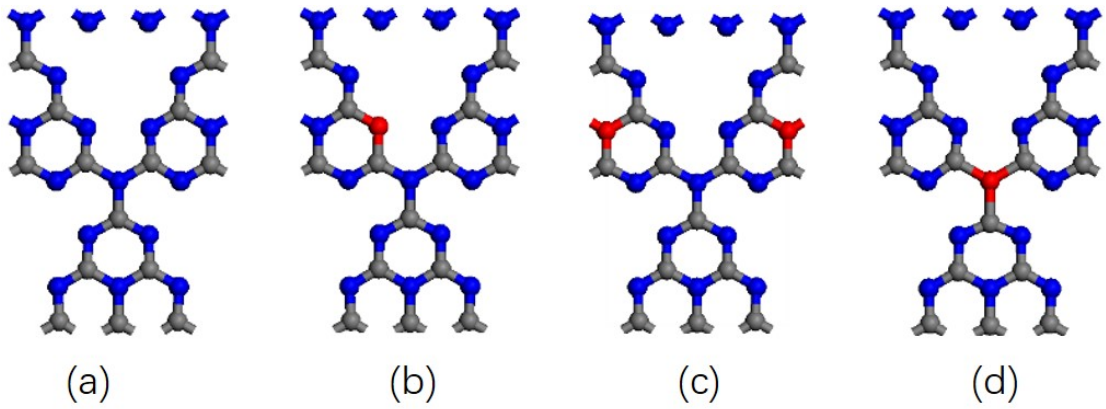

Fig. S6 Doping configuration of mono-oxygen atom at different positions after geometry optimization. (a) to (d) are g-C_3N_4 mono-oxygen atom doping

configurations pre-doping, N1, N2 and N3, respectively (where blue, gray, and red spheres represent C, N, and O atoms, respectively)

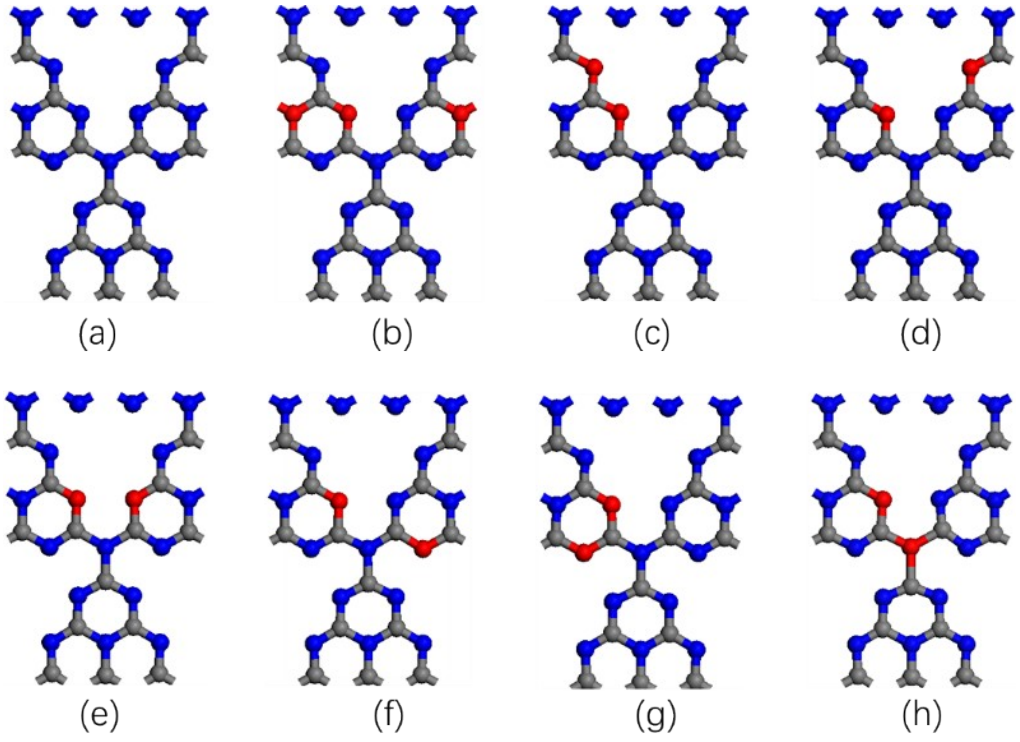

Fig. S7 Geometrically optimized doping configuration of di-oxygen atoms at different positions. (a) to (h) pre-doping, 2', 1' doping, 2', 3' doping, 2', 4' doping, 2', 5' doping, 2', 6' doping, 2', 7' doping, and 2', 8' doped g-C_3N_4 (where blue, gray, and red balls represent C, N, and O atoms, respectively)

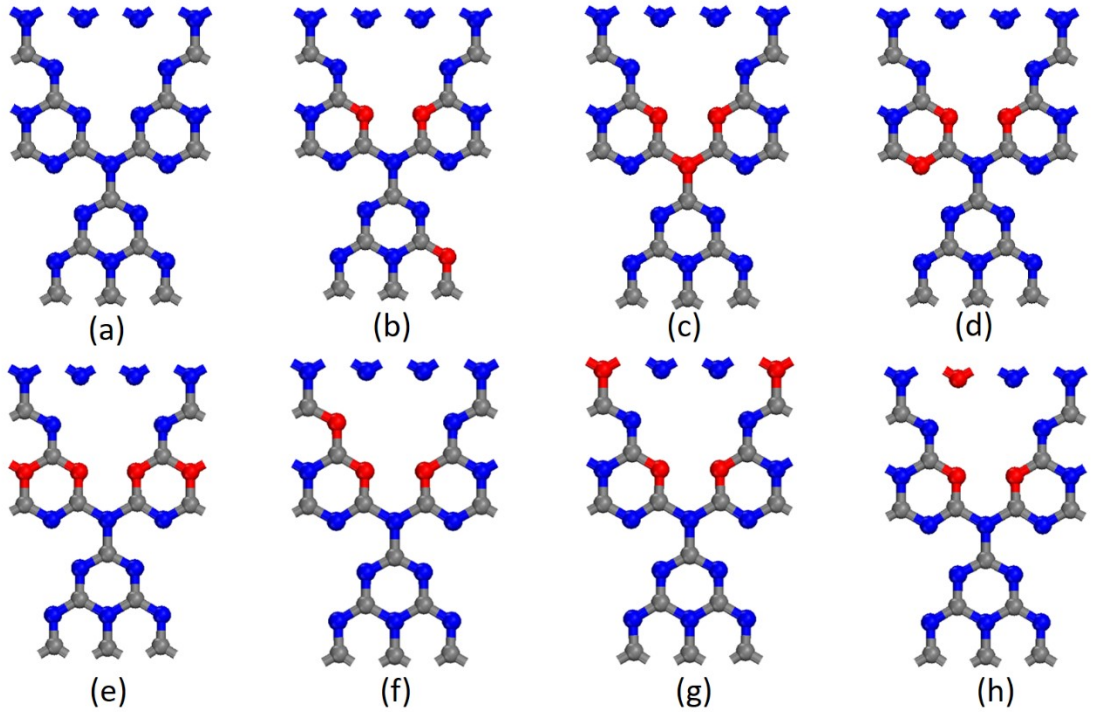

Fig. S8 Geometrically optimized doping configuration of tri-oxygen atoms at different positions. (a) to (h) pre-doping, 2', 2', 1' doping, 2', 2', 3' doping, 2', 2', 4' doping, 2', 2', 5' doping, 2', 2', 6' doping, 2', 2', 7' doping, and 2', 2', 8' doped g-C_3N_4 (where blue, gray, and red balls represent C, N, and O atoms, respectively)

Table S1. The formation energy of mono-oxygen, di-oxygen and tri-oxygen doped g-C_3N_4

mono-oxygen	Energy (eV)	di-oxygen	Energy (eV)	tri-oxygen	Energy (eV)
b	-0.88	b	0.82	a	5.35
c	0.38	c	-1.67	b	1.95
d	1.48	d	-1.93	c	5.37
		e	-2.06	d	1.33
		f	-1.96	e	0.58
		g	-1.58	f	0.65
		f	-1.05	g	3.70

And part of the adsorption configuration before and after geometric optimization are shown as follows.

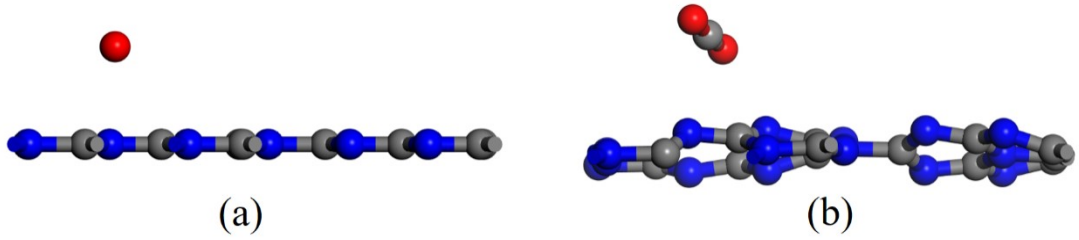

Fig. S9 Schematic diagram of CO_2 adsorption in parallel in a single layer g-C_3N_4 plane

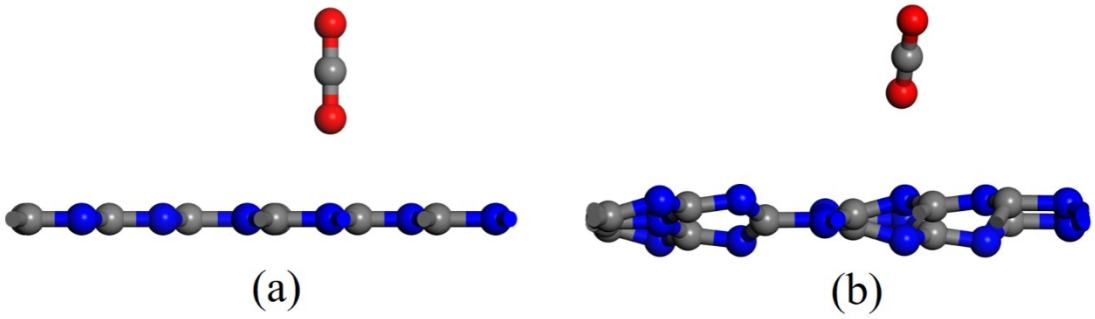

Fig. S10 Schematic diagram of CO_2 adsorption vertically in a single layer g-C_3N_4 plane

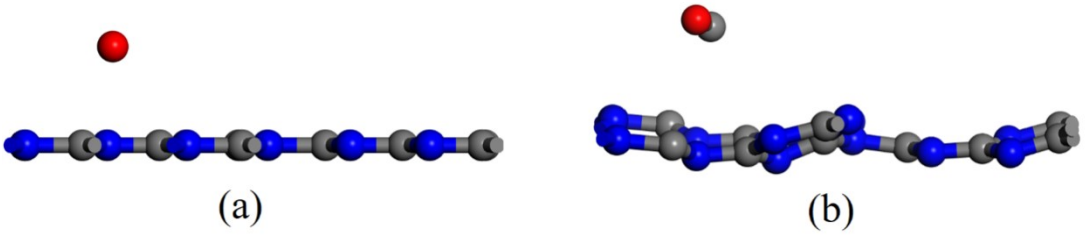

Fig. S11 Schematic diagram of CO adsorption in parallel in a single layer g-C_3N_4 plane

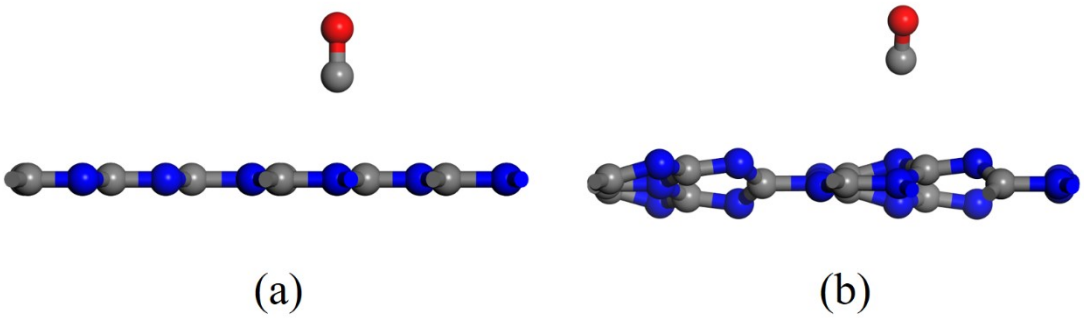

Fig. S12 Schematic diagram of CO adsorption vertically in a single layer g-C_3N_4 plane